Reconstruction of regional mean sea level anomalies from tide gauges using neural networks

Manfred Wenzel,[1] and Jens Schröter,[1]

J. Schröter, Alfred-Wegener-Institute, Bussestr. 24, 27570 Bremerhaven, Germany. (jens.schroeter@awi.de)

M. Wenzel, Alfred-Wegener-Institute, Bussestr. 24, 27570 Bremerhaven, Germany. (manfred.wenzel@awi.de)

[1]Alfred-Wegener-Institute, Bussestr. 24,
27570 Bremerhaven, Germany.

Abstract. The 20th century regional and global sea level variations are estimated based on long term tide gauge records. For this the neural network technique is utilized that connects the coastal sea level with the regional and global mean via a non-linear empirical relationship. Two major difficulties are overcome this way: the vertical movement of tide gauges over time and the problem of what weighting function to choose for each individual tide gauge record. Neural networks are also used to fill data gaps in the tide gauge records, which is a prerequisite for our analysis technique. A suite of different gap filling strategies is tested which provides information about stability and variance of the results.

The global mean sea level for the period January 1900 to December 2006 is estimated to rise at a rate of 1.56±0.25 mm/yr which is reasonably consistent with earlier estimates, but we do not find significant acceleration. The regional mean sea level of the single ocean basins show mixed long term behaviour. While most of the basins show a sea level rise of varying strength there is an indication for a mean sea level fall in the Southern Indian Ocean. Also for the the tropical Indian and the South Atlantic no significant trend can be detected. Nevertheless, the South Atlantic as well as the tropical Atlantic are the only basins that show significant acceleration. On shorter timescales, but longer than the annual cycle, the basins sea level are dominated by oscillations with periods of about 50 to 75 years and of about 25 years. Consequently we find high (lagged) correlations between the single basins.

1. Introduction

Global sea level rise is one of the major concerns in predicting climate and climate change for the decades to come. Projections for sea level rise have been compiled in the IPCC third assessment report [*Church et al.*, 2001] and the more recent 4th report, AR4, [*Bindoff et al.*, 2007]. But still predictions vary substantially. It is important first to understand the magnitude of the past sea level change before we can reduce uncertainties in the future development.

In this paper we will address the development of the global and regional, i.e. ocean basin wide, sea level during the past century. For this purpose monthly mean tide gauge data from the Permanent Service for Mean Sea Level (PSMSL) data base [*Woodworth and Player*, 2003] will be used. However, the question is how well tide gauge records describe regional or global sea level trends. The comparison of altimeter derived sea level change and that at tide gauges indicated that local changes from tide gauges appear to be larger. In recent studies *Holgate and Woodworth* [2004], *White et al.* [2005] as well as *Prandi et al.* [2009] emphasize the differences between the true global mean and the one estimated from tide gauges.

Furthermore processes inside the solid Earth must be considered not only for correcting measurements but also for changes in the shape of the ocean. This leads to the problem of how to separate measured sea level change from local change of the reference system (i.e. land movement). Commonly vertical tide gauge movement is estimated by modelling of the solid earth and its viscous response to past glaciation and mass loading distribution [e.g. *Peltier*, 2004]. Peltier's analysis is available for the whole globe which makes it attractive for use, but many other solutions of the Glacial Isostatic Adjustment (GIA) exist (e.g. *Lambeck and Johnson* [1998], *Milne et al.* [2001], *Mitrovica* [2003] or *Hagedoorn et al.* [2007]). Alternatively, measurements from the Global Positioning System (GPS) at or close to tide gauge locations can be used. This was done thoroughly by various authors like *Teferle et al.* [2006], *Wöppelmann et al.* [2007, 2009] or *Schöne at al.*, [2009]. They all demonstrate local differences between the GIA and GPS solutions.

The question of how to relate tide gauge records to the global sea level was studied by *Church et al.*, [2004]. Only satellite altimetry can provide an almost global mean. *Church et al.*, [2004] used tide gauge records for the last 50 years and related them to the sea level variability and trends measured by the TOPEX/Poseidon mission. The analysis for the period of satellite observations was extended to the past using an Empirical Orthogonal Function (EOF) expansion technique. The EOF method assumes that covariances of the past signal were the same as observed at present. A veritable strength of this method is that the spatial and temporal distribution of tide gauges may change with time. It allowed the reconstruction of the sea level evolution on a spatial resolution of 1 degree globally for five decades. At selected tide gauges an impressive skill could be demonstrated. In a follow on publication *Church and White* [2006], CW06 hereafter, included more historic sea level records and extended the reconstruction back to 1870. CW06 also discuss the error bounds of the analysis and a possible acceleration of sea level rise. In order to relate the relative height of tide gauge locations, which is a difficult geodetic task, *Church et al.* [2004] as well as *Church and White* [2006] performed their analysis in the space of temporal sea level change and later integrated sea level change to sea level height. However, the problem of quality assessment of sea level reconstruction remains an issue.

One way can be comparing the results from alternative approaches because independent measurements are not available.

The relative weighting of the individual tide gauge records is another important task which was tackled by *Jevrejeva et al.*, [2006], J06 hereafter. She and her co-workers carefully studied for which area an individual tide gauge is representative. A weighting scheme was designed that led first to regional and finally to global values. Their scheme is flexible in dealing with gaps in data distribution. J06 cover a somewhat longer period as CW06, i.e. 1807 to present. For long term trends the two estimates of global sea level rise agree reasonably well. *Jevrejeva et al.*, [2008] then provide a thorough discussion of their results concerning dominant periods of variability and their regional distribution, wherein their regions are limited, coastal bound ocean areas.

We try to overcome the serious issues of GIA correction and individual weighting by the use of neural networks, a technique relatively uncommon in oceanography or meteorology, but there are some examples that can be grouped according to their main two application topics: data analysis [*Stogryn et al.*, 1994; *Gross et al.*, 1999; *Müller et al.*, 2003] and prediction [*Wenzel*, 1993; *Tangang et al.*, 1998; *Lee and Jeng*, 2002] among others. Further applications of neural networks in environmental science can be found e.g. in the recent book of *Haupt et al.* [2009].

We will apply the neural network not only to estimate the regional and global sea level change but also to fill temporal data gaps, which is a prerequisite for our method. For gap filling the EOF method is popular, but the weighting of the individual tide gauges remains under discussion. The procedure by J06 could be used as an alternative but is not directly designed for the purpose. However, again the vertical land movement contaminates any estimate.

After a short introduction to neural networks in section 2 we will describe the data used in section 3. A first application of the neural network will be given in section 4 dealing with filling data gaps in the tide gauge records. Finally in section 5 a network will be applied to estimate the regional mean sea level and section 6 will give a short summary.

2. The Neural Network

A neural network is an artificial neural system, a computational model inspired by the notion of neurophysical processes. It consists of several processing elements called neurons, which are interconnected with each other exchanging information. There are many different kinds of such neural networks which differ in the way the neurons are interconnected and in the way the single neurons behave. A detailed overview can be found e.g. in the books of *Freeman and Skapura* [1991] or *Bishop* [1995, 2006].

In this paper a *backpropagation network* (BPN) will be used. This type of network is mainly used for tasks like classification and pattern recognition in noisy environments or for data compression/decompression purposes. The BPN was first formulated by *Werbos* [1974] and later by *Parker* [1985]. In this type of network the neurons are ordered into layers: an input layer on the top, one or more hidden layers below and an output layer at the bottom. In addition to the neurons there is a bias element in the input and the hidden layer(s) that has no input but a constant unique output value. The information propagates forward through the network from the input to the hidden layer(s) and then to the output. To manage this, each neuron (including the bias) of one layer is connected to every neuron in the underlying layer. They are not interconnected within the layers and there is no feedback. Each connection can be characterized by a certain connection strength or weight. The neurons of the input layer usually do only a scaling transformation on the input data, while the neurons in the following layers can be divided into two sections: an input section that sums the incoming signals from the overlying layer using the individual weights and a transfer/output section where the resulting signal is modified by a transfer function $\mathcal{F}\{\}$. Thus the output y_k of the neuron k in dependence to its input $\{x_i\}$ can be described as:

$$y_k = \mathcal{F}\{b_k + \sum_{i=1}^{N} W_{k,i}\ x_i\}$$

where N gives the number of neurons in the layer above, $W_{k,i}$ is the connection strength/weight matrix and b_k the corresponding bias. An appropriate choice of the transfer function in the hidden layer is a sigmoid function, which is differentiable, output-limiting and quasi-bistable. Thus these neurons work like switches.

In a first test experiment aimed at filling data gaps in the tide gauge records (see section 4) we applied a BPN with the hidden layer divided into three sections with different transfer functions $\mathcal{F}\{\}$. In the first section we used $\mathcal{F}\{x\} = 1/(1+\exp\{-x\})$, in the second $\mathcal{F}\{x\} = \tanh\{x\}$ and in the third a linear transfer $\mathcal{F}\{x\} = x$. After training the BPN we found that only connections going through hidden neuron with either $\mathcal{F}\{x\} = \tanh\{x\}$ or $\mathcal{F}\{x\} = x$ contribute to the output signal. Therein the connections crossing the linear hidden neurons can be re-written as direct connections from the input to the output layer. Therefore we decided to use in this paper a general neural network(s) design as illustrated in Fig. 1 with $\mathcal{F}\{x\} = \tanh\{x\}$ for the hidden neurons and a linear transfer, $\mathcal{F}\{x\} = x$, for the output neurons, which results in the full network equation:

$$\vec{y} = \vec{b_O} + \mathbf{W}_{IO} \cdot \vec{x} + \mathbf{W}_{HO} \cdot \tanh\{\vec{b_H} + \mathbf{W}_{IH} \cdot \vec{x}\} \quad (1)$$

The amount of neurons in each layer will be chosen depending on the special task. Note that (1) describes a hybrid approach: setting $\mathbf{W}_{HO}$ to zero leads to linear regression while $\mathbf{W}_{IO} = 0$ retrieves the original description of a backpropagation network.

The matrices of the connection strength between the neurons from the different layers ($\mathbf{W}_{IO}$: direct input to output, $\mathbf{W}_{IH}$: input to hidden and $\mathbf{W}_{HO}$: hidden to output) as well as the bias terms $\vec{b_H}$ and $\vec{b_O}$ are unknown initially and will be estimated in a training phase, i.e. the BPN learns from given examples (*supervised learning* in the terminology of neural networks). Given a set of M known training vector pairs $\{\vec{x}_m^{dat}, \vec{y}_m^{dat}\}$, i.e. input and associated output vectors (target values), we minimize the quadratic error E at the output of the network:

$$E = \frac{1}{2} \sum_{m=1}^{M} \sum_{k=1}^{K} \left(y_k^{net}(\vec{x}_m^{dat}) - y_{k,m}^{dat} \right)^2 \tag{2}$$

where the summations include all K output neurons and all M training pairs. To find the minimum of E an iterative gradient descent algorithm will be applied. The necessary gradient of E with respect to the unknown weights $\mathbf{W}_{IO}$, $\mathbf{W}_{IH}$ and $\mathbf{W}_{HO}$ as well as to the biases $\vec{b_H}$ and $\vec{b_O}$ can easily been derived from (1) and (2) using the chain rule. The optimizations done in the following sections will all start from small random numbers in the range [-0.01,+0.01] as a first guess for the unknowns and we will allow for a maximum of 500 iterations.

In oceanographic and meteorological applications one often has to deal with a large number of input as well as output neurons, which results in a huge amount of parameters (N_{par}) to be estimated. Usually there will be only a much smaller set M of training examples leading to an ill-conditioned problem [*Hsieh and Tang*, 1998]. Because of the non-linearity of the hidden neurons transfer function many local minima of the costfunction E exist. To moderate the danger of getting trapped in one of these local minima *Freeman and Skapura* [1991] propose to enlarge the training data set by including examples with noise added to the input. This procedure was successfully applied by *Wenzel* [1993] and we will follow this line in this paper.

Furthermore, the situation $M \ll N_{par}$ might lead to an overfitting of the neural network, i.e. the network looses its capability to generalize and the error will be unnecessarily high when applying the network to examples not used for training. To overcome this problem *Tangang et al.* [1998, their appendix] suggest to add a penalty term to (2) that forces unimportant weights to approach zero (auto pruning, ridge regression):

$$R = \frac{1}{2}\left[C_{IO}\sum w_{IO}^2 + C_{IH}\sum w_{IH}^2 + C_{HO}\sum w_{HO}^2\right] \qquad (3)$$

with positive constant factors C_{IO}, C_{IH} and C_{HO}. The summations include all elements w of the corresponding matrix $\mathbf{W}_{IO}$, $\mathbf{W}_{IH}$ and $\mathbf{W}_{HO}$, respectively. To simplify the optimal choice of the factors C_j (the subscript j denotes the corresponding matrix) we rewrite them in the form:

$$C_j = C_r \cdot K \cdot M/N_j \qquad (4)$$

with N_j giving the corresponding number of matrix elements. Thus finally only the single constant C_r has to be choosen. We will come back to this later according to demand.

3. Data

For our purpose we use monthly sea level data from tide gauges downloaded from the Permanent Service for Mean Sea Level (PSMSL) website [http://www.pol.ac.uk/psmsl] in June 2008. To avoid possible problems with the different local reference frames all computations will be done in the space of temporal derivatives, i.e. monthly differences.

Beyond that, this makes the data more suitable for the BPN because it better limits the possible range of the numerical values. To reduce the noise in the temporal derivatives all time series are smoothed prior to further processing using a Gaussian filter, $\exp\{(t-t_0)/t_{sm}\}^2$ with $t_{sm} = 2.5$ month width.

From the PSMSL sea level data all tide gauges with revised local reference (RLR data) are selected that comply with the following conditions: (i) there are more than 11 annual mean values given in [1993,2005], (ii) more than 50 annual mean values are given in [1900,2006] and (iii) they are not located in the Mediterranean, North or Baltic Sea. Multiple records near a $1°\times 1°$grid point are averaged to one. This results in a set of 56 tide gauges (Fig. 2). Although every tide gauge has more then 50 years of data, many values are missing, especially prior to 1950 (Fig. 3). We will deal with this point in section 4. The selected tide gauges are GIA corrected using the ICE-5G model [*Peltier*, 2004] version VM4 downloaded also from the PSMSL website [http://www.pol.ac.uk/psmsl/peltier/index.html]. Incidentally this correction is not really necessary as one can deduce it from the structure of the BPN. Any linear transformation of the BPN input signal can be mapped as part of the related weights and biases.

The main purpose of this paper is to estimate regional mean sea level anomalies (regional MSLA's) from this set of selected tide gauges directly using a neural network. To train such a network corresponding regional mean target values are needed. For the period from 1993 onward these values can be derived from the satellite altimetric measurements. We will use either the TOPEX/Poseidon data processed by GFZ Potsdam [T.Schöne, S.Esselborn pers. communication] and / or the combined

TOPEX/Poseidon and Jason-1 sea level fields available at the CSIRO sea level webpage [http://www.cmar.csiro.au/sealevel/sl_data_cmar.html]. Due to differences in processing the satellite data these products are distinct from each other not only locally but also for the regional means. Table 1 gives the temporal root mean square (RMS) values of these differences for the ocean regions considered in this paper (color shaded areas in Fig. 2). Compared to the RMS value of the signal they are most pronounced in the tropical belt (15°S–15°N), as e.g. in the tropical Pacific (Fig. 4a), and are also notable in the global mean (Fig. 4b).

4. Filling Data Gaps

A neural network needs complete information at the input layer to fulfill its duty, but from Fig. 3 we see that there are many tide gauge data missing. When applying a neural network to estimate the regional MSLA's from the tide gauges the simplest way out seems to fill the gaps by some dummy value. To handle this the BPN has to be trained accordingly, i.e. the training data set has to include all possible configurations of gaps, which would make the training unnecessarily complicated. A better way is to use more sophisticated methods to fill the gaps. Several alternatives (Table 2) are tested / used here. This includes the replacement of the missing values by the mean annual cycle (MAC) of the corresponding tide gauge as well as the reconstruction using an EOF basis estimated from all timesteps that have a complete tide gauge dataset (EOFR).

Furthermore a *forecast network* (FCnet) is built, that is trained to compute the values at all tide gauge positions for timestep (n+1) from all values at the steps (n) and (n-1). Additionally an equivalent *backcast network* (BCnet) is constructed that computes the values for step (n-1) from the steps (n) and (n+1). Thus these networks act as time stepping operators. Both networks have the following dimension: 112 input, 84 hidden and 56 output neurons, i.e. there are 20524 parameters / weights to estimate. The networks are trained using all 297 examples that have three complete subsequent timesteps.

Following the suggestion of *Freeman and Skapura* [1991] examples with noise added to the input are included in the training to moderate the problem of getting trapped in local costfunction minima. Each of the original training examples is repeated three times with Gaussian noise added that corresponds to 5, 10 and 15%, respectively, of the standard deviation estimated from all utilized tide gauge values.

To tackle the problem of overfitting, the ridge regression penalty (3) is included in the training of the networks. To find an appropriate value of C_r we tested the values 0 to 50 in steps of 10. Figure 5 shows the dependence of the BCnet output error on the choice of C_r. Here the BCnet is applied recurrently starting from February, 2007 going backwards in time, i.e. data gaps at the input of the BCnet are filled using the output from the previous step(s). To start this time stepping procedure, data gaps at the very beginning are filled with values taken from the mean annual cycle. The benefits of (3) are obvious: Compared to not applying the ridge regression penalty ($C_r = 0.0$) the error of the network output is reduced by about 25% in unknown environments, i.e. for timesteps not used in the training phase (mainly before 1955), while the error gets only slightly worse for the training examples (the minimum values in Fig. 5 after 1955). There is only weak dependence on the actual value of C_r but we found a slight minimum for $C_r = 30$. A further increase of C_r worsens the error again for untrained examples. Analogous results are found for the FCnet. This induces the final choice of $C_r = 30$.

As an example Fig. 6 shows the reconstructed sea level derivatives at the tide gauge Kwajalein (code 720011, position: 8.73°N 167.73°E) for the period 1940–1960. Alternatively to using the FCnet and the BCnet recurrently (Fig. 6a) we also tested the combination of the neural network and the MAC/EOFR reconstruction, i.e. we filled the data gaps at the network input by taking values either from the MAC (Fig. 6b) or from the EOFR (Fig. 6c). All reconstructed time series reproduce the original data resonably well and have approximately the same error when compared to all known data points (Fig. 7). For both networks the RMS of the output error is lowest at the timesteps used for training. At untrained timesteps after $\sim$1940 it stays at the level of about 40% the standard deviation estimated from the existing tide gauge data at the corresponding timestep. With the increasing number of data gaps before 1940 the error slightly rises to about 60%. When filling the gaps with the MAC (Tab. 2, case 1) the error stays at the 60% level after 1940 and rises to about 100% before (Fig. 7a). For EOFR (Tab. 2, case 2) the error appears much less because the EOF method minimizes the error at given data points directly.

From these results it is hard to distinguish which reconstruction to prefer, and in the following we will treat all timeseries as an ensemble of possible realisations. The ensemble is enlarged by two further realisations: one takes the best of the single network reconstructions (Tab. 2, cases 3 to 8) at each timestep, i.e. the one with minimum error, and the other is built as the error weighted mean of the these. Using this ensemble will allow us later on to account for the uncertainty in the reconstruction and to do some error statistics.

5. Regional Mean Sea Level

5.1. Reconstruction

The final purpose of this paper is to estimate the regional MSLA for the eight ocean regions that are indicated by color shading in Fig. 2. This will be done by using a neural network that is supplied with the monthly difference values from all selected tide gauges and gives the corresponding regional MSLA derivatives for all the ocean regions at once. This network will be denoted as TGRMnet in the following. Again we utilize a BPN of the same general configuration as in section 4. In this case the network has 56 input neurons, i.e. one for each tide gauge, and eight output neurons, i.e. one for each ocean region. To complete the network layout there are 112 hidden neurons implemented. This finally gives 7736 connection weights to be estimated. Note that there is no extra output neuron for the global MSLA! Instead, the network training includes an additional constraint that minimizes the difference between the area weighted mean of the regional MSLA from the network and the corresponding given global value. Prior experiments have shown that this procedure results in more robust estimates because it interlinks the output neurons.

The TGRMnet is trained using three alternatives of regional MSLA data: the corresponding values are computed either from the GFZ altimetry data (GFZ-training) or from the CSIRO dataset (CSIRO-training). In the third case we use both datasets simultaneously (CSIRO+GFZ-training), i.e. there are two different target values for the same BPN input. The temporal overlap with the tide gauges ranges from Jan.1993 to Jun.2005. Thus there are 148 basic examples available to train the network (this number doubles in case of the CSIRO+GFZ-training). As for the training of the FCnet and BCnet (section 4) we increased this number by adding training examples with noisy input to moderate the problem of getting trapped in local costfunction minima. Using two different target values for the same input as in the CSIRO+GFZ-training is somewhat like adding noise to the output too. This interpretation leads to a further difference in the BPN training as compared to the common standard: the misfit at the output neurons will be weighted according to the uncertainty of the training data, i.e. the final costfunction E for the TGRMnet is:

$$\begin{aligned} E_m &= \frac{1}{2}\sum_{k=1}^{K} rw_k \ \left(y_k^{net}(\vec{x}_m^{dat}) - y_{k,m}^{dat}\right)^2 \\ &+ \frac{1}{2} rw_{glob} \left[\left(\sum_{k=1}^{K} A_k \ y_k^{net}(\vec{x}_m^{dat})\right) - y_{glob,m}^{dat}\right]^2 \\ E &= \sum_{m=1}^{M} E_m + R \end{aligned} \tag{5}$$

where $\sum_k$ adds up the ocean regions and A_k are the weights (relative areas of the ocean basins) to compute the global value from the regionals. R is given by (3). The RMS of the difference between the GFZ and the CSIRO data (Tab. 1) give a reasonable approximation for the data uncertainty and the weights of the regional misfits, rw_k, are the squared inverse of the corresponding RMS values. They are applied for all three training datasets.

To estimate the weight C_r of the ridge regression penalty (Eq. 3 and 4) we scanned the range 0 to 500 and performed a fivefold cross-validation on the training dataset(s) following *Cannon and Hsieh* [2008]. However, we did not perform a second validation loop as in *Cannon and Hsieh* [2008]. For the cross-validation the training data are split into five continuous segments. The TGRMnet's are trained on four of these segments while the data from the fifth segment are retained for validation. In a sixth cross-validation case we retain 20% of the data that are randomly chosen from the complete training dataset.

Figure 8 shows the dependence of the cost E_m (5), converted to a mean RMS error, on the validation case and on C_r. The results are very similar for all validation cases. When applying the networks to the data used for training the remaining error increases with increasing C_r, but it stays well below the data uncertainty. Applying the networks to the data retained for validation the error is about twice the data uncertainty, except for validation case six where it is about the same size. The random choice of retained data obviously leaves a better coverage of known input/output situations for training than the continuous segments. The closer unknown situations are to the ones used for training the better a neural network performs there. Anyhow, although C_r values with minimum error can be identified in each case (marked by the stars on the x-axis) there is no clear dependence. Thus we retrained the networks using the complete data with these C_r values that give minimum error. That are: 1., 2.5, 5., 7.5, 300 for the CSIRO-training; 0., 1., 2.5, 7.5, 250. for the GFZ-training and 0., 1., 5., 200., 500. for the combined CSIRO+GFZ-training. This gives fifteen versions of the TGRMnet. This procedure is certainly good enough to estimate reasonable C_r values, but whether it is sufficient to estimate the uncertaincy of the final TGRMnet's is under debate, because they can no longer be validated against independent data. However, one may assess their errors from the validation cases. By using the ensemble of differently trained networks and taking the mean of the output afterwards we follow the recommendation of e.g. *Tangang et al.* [1998] to improve the quality.

All fifteen versions of the TGRMnet in combination with all ten tide gauge reconstructions (Tab. 2) are used to estimate the regional mean sea level derivatives (monthly differences) for the time 1900-2006. This results in an ensemble containing 150 members.

Each member is then converted to regional MSLA by temporal integration, i.e. building the cumulative sum. An offset is added to all these regional MSLA curves to obtain a zero temporal mean in 1993-2005.

Figure 9 shows the resulting MSLA for the sub-ensembles of the CSIRO and GFZ trained networks, i.e. taking the results from all C_r values and from all tide gauge reconstructions (=50 members), compared to the corresponding training data. The global ocean and the North Pacific are taken as examples. The training data are well reproduced by the TGRMnet although there are deviations noticeable especially for the global ocean (Fig. 9a). These are mainly caused by the apparent differences in the overall trends of the TGRMnet and the training data. However, the differences are smaller than those between the observations (Tab. 1, column *diff*). Furthermore, the maximum deviations from the corresponding data stay at or even below the the standard deviation of the difference between the two training data sets. Similar results are obtained for the regions not shown. Good agreement with the training data we find also for the amplitude and phase of the annual cycle. After high-pass filtering the MSLA timeseries (using a 1.5 years cut-off frequency) the amplitude and phase are estimated by fitting an annual sinusoid. To get an idea about its temporal variability this is done in a moving five year window. The agreement is demonstrated in Fig. 10 for the global ocean. As good or even better results are found for the single ocean basins.

5.2. Discussion

First we looked at the dependence of the regional MSLA on the dataset chosen for training (Fig. 11). The interannual to multi-decadal variablity shows only minor dependence on the training data. The influence of the data is mainly noticeable in the mean trends given in Tab. 3 (ensemble means and standard deviations). At the first glance there seems to be no systematic behavior for the difference between the regional MSLA trends derived from the GFZ and the CSIRO trained networks. More detailed inspection shows that it depends on the difference in the trends of the data during the training period. An unforeseen result was obtained for the global MSLA, the North Pacific, the North Atlantic and the South Atlantic (Fig. 11a, d, g and i respectively): the regional MSLA curves from the CSIRO+GFZ training does not inevitably stay between the curves obtained from the GFZ and the CSIRO training for the whole time. The reason for this is not clear yet.

In the following we will discuss only the mean sea level curves estimated from the complete 150 member ensemble. On longer timescales (after low-pass filtering using a 1.5 year cut-off frequency) the global MSLA (Fig. 11a) exhibits only little variations as compared to the regional MSLA. Our global MSLA shows more similarities to the one of *Holgate* [2007], estimated from only a small number of tide gauges, than to the results obtained by CW06 or J06. The largest deviations of our global MSLA from CW06 or J06 appear prior to 1950. For this period the amount of available information from tide gauges is drastically reduced as compared to the second half of the century. Thus these differences in the global MSLA are obviously due to the different treatment of this situation.

In any case, our estimate of the global mean sea level trend (1.56±0.25 mm/yr, Tab. 3) fits well to the 20th century sea level rise estimates of *Hagedoorn et al.* [2007] (1.46±0.2 mm/yr, using GIA corrected tide gauges) or *Wöppelmann et al.* [2009] (1.61±0.19 mm/yr, using GPS corrected tide gauges). These values are in between an earlier estimate of *Wöppelmann et al.* [2007] (1.31±0.3 mm/yr), *Holgate* [2007] (1.74±0.16 mm/yr) and the ones obtained by CW06 and J06, 1.7±0.3 mm/yr and

1.8 mm/yr, respectively, wherein our estimate using only the GFZ trained networks (1.39±0.30 mm/yr) corresponds better to the estimate of *Wöppelmann et al.* [2007] while the trend resulting from the CSIRO training (1.68±0.16 mm/yr) fits better to CW06.

Within this range of values the estimate of J06 might be seen as an upper limit. For the period 1993–2002 *Holgate and Woodworth* [2004] found that during the 1990s the *global coastal mean sea level* derived from tide gauges increased faster than the global average sea level from altimetry. This finding was confirmed by *White et al.* [2005] for the 1990s and around 1970 based on the sea level reconstructions of *Church et al.* [2004]. However, *White et al.* [2005] did not find any significant difference between the globally averaged and the coastal sea level trend when looking at their full reconstruction period, 1950–2000.

Compared to the global mean the regional sea levels within the single ocean basins behave quite differently: In the Indian Ocean the tropical MSLA (Fig. 11b) is dominated by a multi-decadal oscillation with a rather positive mean trend (0.65±0.81 mm/yr, Tab. 3) and negative acceleration (–0.0094±0.0105 mm/yr^2, Tab. 4) while it is the other way round for the Southern Indian Ocean (Fig. 11c) that shows a sea level fall (–0.59±0.72 mm/yr) and positive acceleration (0.0064±0.0112 mm/yr^2). In contrast to this difference in the very long timescale the shorter scales in these basins are well correlated. After eliminating the annual cycle and subtracting the corresponding quadratic regression lines from the sea level curves (Fig. 12a) the correlation is 0.6, with the Southern Indian Ocean leading by 14 months (Note: all correlations given hereafter are significant at the 99% level).

For the Pacific Ocean (Fig. 11d-f) the variations in the single sub-basins are even more similar. All basins show a distinct linear sea level rise with the highest rate in the northern basin (3.25±1.22 mm/yr) and the lowest in the southern (1.23±0.66 mm/yr). None of the Pacific basins show significant acceleration. After subtracting the quadratic regression lines (Fig. 12b) we find a dominant oscillation with a 70 year period (period estimated via auto-correlation) for the North as well as for the tropical Pacific. The correlation among each other is 0.8 with the tropical Pacific leading by about 44 years, i.e. these basins are approximately in anti-phase. Lower (absolute) correlations are found for these basins with the South Pacific: 0.6 for the North (South Pacific leads by ∼43 year) and –0.7 for the tropical Pacific (South Pacific leads by ∼48 years). These reduced correlations are caused by the relatively strong oscillation on shorter timescales (∼25yr) visible in the South Pacific.

In the Atlantic Ocean (Fig. 11g-i) the sea level changes are dominated by a rise in the northern basin (3.70±1.11 mm/yr) and in the tropics (2.51±0.73 mm/yr) while there is no trend at all in the southern basin during the full reconstruction period (0.00±0.77 mm/yr). Significant acceleration of sea level rise is only found for the tropical Atlantic (0.0115±0.0084 mm/yr^2) and for the South Atlantic (0.0233±0.0127 mm/yr^2). After subtracting the quadratic regression all Atlantic basins (Fig. 12c) are dominated by multi-decadal variations, that exhibit main periods of approximately 23 and 65 years. Thereby the 23 year period is most pronounced in the North Atlantic while the 65 year period is mainly noticeable in the South. Consequently we find strong cross-correlations among the single ocean basins in the Atlantic too: –0.69 between the tropical Atlantic and the South Atlantic (tropical Atlantic leads by ∼23 years), 0.66 between the tropical Atlantic and the North Atlantic (North Atlantic leads by ∼44 years) as well as 0.65 between the North Atlantic and the South Atlantic (North Atlantic leads by ∼38 years).

Beside these interbasin cross-correlations we also find good lag correlations at long timescales between the regional MSLA's and external indices, especially the Pacific Decadal Oscillation (PDO), that is the leading principal component of the monthly sea surface temperature (SST) anomalies in the North Pacific Ocean poleward of 20°N [*Mantua et al.*, 1997], and the Southern Annular Mode Index (SAM), which is defined as the difference in the normalized monthly zonal mean sea level pressure between 40°S and 70°S [*Nan and Li*, 2003]. The correlations with the PDO are e.g. -0.6 for the North Pacific, that leads the PDO by ∼9 years, and -0.5 for the tropical Pacific, that lags by 26 years. Similar phase lags but with reduced correlations are obtained using the Interdecadal Pacific Oscillation Index (IPO; *Parker et al.* [2007]). Best correlations with the SAM (∼0.5) are found for the southern hemisphere ocean basins and for the global ocean. We also see similarities with the multidecadal SST modes derived by *Mestas-Nuñez and Enfield* [1999] especially for the North Atlantic (their Fig. 1) but also for the tropical Pacific (their Fig. 4) and the North Pacific (their Fig. 5). All this indicates the importance of the changes in ocean temperature as well as in ocean circulation (wind forcing) on the regional sea level. However, these are not the only influences. On regional scale the halosteric effects cannot be neglected (e.g. *Wenzel and Schröter* [2007]).

Finally, we look at the annual cycle of the regional MSLA. The good agreement between the TGRMnet results and the corresponding training data (Fig. 10) encourages us to look at the whole period from 1900 onward that is displayed in Fig. 13. The amplitudes of the annual cycle (Fig. 13a, b and c) show substantial temporal variations in the single ocean basins in dependence of its mean value. In contrast to this the phases (Fig. 13d, e and f) appear to be quite constant except for the tropical regions. Here the phase may vary by up to 4 month (e.g tropical Pacific). The highest annual amplitudes are found for the northern hemisphere basins (3.30±0.24 cm for the North Atlantic and 2.67±0.20 cm for the North Pacific) with the maximum sea level appearing in late September, early October. Amongst the southern ocean basins the annual amplitudes appear to be more similar (1.33±0.18 cm, 1.18±0.10 cm and 1.21±0.12 cm for the South Atlantic, Pacific and Indian Ocean, respectively) with the maximum sea level at the end of the austral summer. Furthermore we find phase differences among the southern basins: the South Pacific is lagging the Southern Indian Ocean and the South Atlantic by about 0.7 month and 1.1 month, respectively. The lowest annual amplitudes are found for the tropical basins (0.56±0.11 cm, 0.18±0.08 cm and 0.45±0.11 cm for the tropical Atlantic, Pacific and Indian Ocean, respectively) and they are even lower for the global ocean (0.24±0.03 cm).

6. Summary and Conclusions

In this paper we demonstrated the feasibility and usefulness of neural networks within two different applications: filling data gaps in the tide gauge timeseries and in estimating the evolution of regional mean sea levels from these tide gauge data. First some general remarks about the networks: they are easy to use and appear to be an appropriate tool for the tasks in this paper, even though they have their disadvantages. In unknown environment, i.e. outside the training period, the behaviour of a neural network strongly depends on the way it has been trained, to what extent it has learned to generalize. This has been demonstrated in connection with both applications, the gap filling (section 4) as well as the reconstruction of the regional sea levels (section 5.1). To improve the quality of the network output it is recommended to use an ensemble of differently trained networks (e.g. *Tangang et al.* [1998]) and to take the mean afterwards. Further but usually minor drawbacks are: neural networks are not very flexible, i.e. once they are trained the user is fixed to the chosen input / output configuration, and it is hard to impossible to learn from the network about e.g. the underlying mathematics or physics. For instance, one example for the latter is related to the GIA correction of the tide gauges. Although we applied this correction, it was not really necessary when estimating the regional MSLA from tide gauges. All computations are done in the space of temporal derivatives, i.e. monthly differences, and any additive correction to the input (tide gauge) signals needed, whether it stems from the global isostatic adjustment or from any other secular vertical land movement, would appear as a contribution to the bias of the hidden neurons. On the one hand this is an advantage of using the neural network, but on the other hand it is impossible to extract details about the correction made for a single tide gauge. Anyhow, another great advantage of the neural network is, that there is no need to determine the weighting of the individual tide gauges. The network learns during the training which weights are appropriate. It also learns which tide gauge is most appropriate for which ocean basin.

Information from 56 selected tide gauges are used to estimate the regional MSLA for the years 1900 to 2006. Although every tide gauge has more then 50 years of data, many values are missing, especially prior to 1950 (Fig. 3). This rapidly decreasing amount of direct information from the tide gauges back in time would cause problems for any method applied to estimate the mean sea level and result in increasing errors. In order to reduce these errors we first filled the data gaps in a reasonable way by neural networks that simulate the temporal evolution of all selected tide gauges at once by integrating either forward or backward in time.

The reconstructed regional MSLA of the single ocean basins significantly differ in the long term behaviour that can be approximated by quadratic regression (see Tab. 3 and 4). While most of the basins show a sea level rise of different strength there is a mean sea level fall in the Southern Indian Ocean and no significant trend can be detected in the tropical Indian and the South Atlantic. Nevertheless, the South Atlantic as well as the tropical Atlantic are the only basins with significant acceleration. For the global mean sea level we estimate a trend of $+1.56 \pm 0.25$ mm/yr. This value fits well to the earlier estimates of CW06 (1.7 ± 0.3 mm/yr), J06 (1.8 mm/yr), *Hagedoorn et al.* [2007] (1.46 ± 0.2 mm/yr) or *Wöppelmann et al.* [2009] (1.61 ± 0.19 mm/yr). In contrast to CW06 or J06 we did not find any significant acceleration in sea level rise. This is obviously due to the missing depression in sea level prior to 1950 that is the main difference of our result to CW06 and J06 (Fig. 11a).

On medium timescales, i.e. after eliminating the annual cycle and subtracting the quadratic regression, the estimated regional mean sea levels are dominated by oscillations with periods of about 50 to 75 years and $\sim$25 years (the latter especially in the South Pacific). Consequently there are high phase lagged correlations among the basins. Good correlations also exist with external indices like the PDO and SAM. Furthermore, the timing of the annual maximum in the northern and southern ocean basins at the end of their hemispherical summer indicates the importance of the thermosteric contribution to the (seasonal) sea level variation. This lets us conclude that the estimated variations show some realism. They are not only due to steric effects and/or the regional freshwater balance. There must also be periodic mass exchange between the single basins not only at seasonal periods [*Stammer et al.*, 1996; *Ponte*, 1999] but also on longer time scales as proposed e.g. by *Stepanov and Hughes* [2006] or *Wenzel and Schröter* [2007]. Anyhow, to figure this out in more detail is beyond the scope of this paper and information about the steric contribution during the whole reconstruction period would be needed at least.

Acknowledgments. The authors wish to thank the anonymous reviewers for their fruitful comments that helped to improve the paper.

References

Bindoff, N.L., J. Willebrand, V. Artale, A, Cazenave, J. Gregory, S. Gulev, K. Hanawa, C. Le Quéré, S. Levitus, Y. Nojiri, C.K. Shum, L.D. Talley, and A. Unnikrishnan (2007), Observations: Oceanic Climate Change and Sea Level. In: *Climate Change 2007: The Physical Science Basis. Contribution of Working Group I to the Fourth Assessment Report of the Intergovernmental Panel on Climate Change* [Solomon, S., D. Qin, M. Manning, Z. Chen, M. Marquis, K.B. Averyt, M. Tignor and H.L. Miller (Eds.)], Cambridge University Press, Cambridge, United Kingdom and New York, NY, USA., pp. 385–432.

Bishop, C.M. (1995), Neural Networks for Pattern Recognition, *Clarendon Press*, Oxford, pp. 482.

Bishop, C.M. (2006), Pattern Recognition and Mashine Learning, *Springer*, New York, pp. 738.

Cannon, A.J., and W.W. Hsieh (2008), Robust nonlinear canonical correlation analysis: application to seasonal climate forecasting. *Nonlin. Processes Geophys.*, *15*, 221–232.

Church, J., J. Gregory, P. Huybrechts, M. Kuhn, K. Lambeck, M. Nhuan, D. Qin, and P. Woodworth (2001), Changes in sea level. In *Climate Change 2001: The Scientific*

Basis, Contributions of the Working Group I to the Third Assessment Report of the Intergovermental Panel on Climate Change [J. T. Houghton, Y. Ding, D.J. Griggs, M. Noguer, P. J. van der Linden and D. Xiaosu (Eds.)], Cambridge University Press, New York, pp. 641–684.

Church, J.A., N.J. White, R. Coleman, K. Lambeck, and J.X. Mitrovica (2004), Estimates of the Regional Distribution of Sea Level Rise over the 1950 to 2000 Period. *J. Clim.*, *17*, 2609–2625.

Church, J.A., and N.J. White (2006), A 20th century acceleration in global sea-level rise, *Geophys. Res. Lett.*, *33*, L01602, doi:10.1029/2005GL024826 .

Freeman, J.A., and D.M. Skapura (1991), Neural Networks – Algorithms, Applications and Programming Techniques, *Addison-Wesley Publishing Company*, Reading, MA, pp. 401.

Gross, L., S. Thiria, and R. Frouin (1999), Applying artificial neural network methodology to ocean color remote sensing, *Ecological Modelling*, *120*, 237–246, doi:10.1016/S0304-3800(99)00105-2 .

Hagedoorn, J.M., D. Wolf, and Z. Martinec (2007), An estimate of global mean sea-level rise inferred from tide-gauge measurements using glacial-isostatic models consistent with the relative sea-level record, *Pure Appl. Geophys.*, *164*, 791–818, doi:10.1007/s00024-007-0186-7

Haupt, S.E., A. Pasini and C. Marzban (2009), Artificial Intelligence Methods in the Environmental Sciences, *Springer Verlag*, Berlin, Heidelberg, pp. 424

Holgate, S. J. (2007), On the decadal rates of sea level change during the twentieth century, *Geophys. Res. Lett.*, *34*, L01602, doi:10.1029/2006GL028492

Holgate, S.J., and P.L. Woodworth (2004), Evidence for enhanced coastal sea level rise during the 1990s, *Geophys. Res. Lett.*, *31*, L07305, doi:10.1029/2004GL019626

Hsieh, W.W., and B. Tang (1998), Applying Neural Network Models to Prediction and Data Analysis in Meteorology and Oceanography. *Bull. Amer. Meteor. Soc.*, *79*, 1855–1870.

Jevrejeva, S., A. Grinsted, J.C. Moore, and S. Holgate (2006), Nonlinear trends and multiyear cycles in sea level records, *J. Geophys. Res.*, *111*, C09012, doi:10.1029/2005JC003229

Jevrejeva, S., J.C. Moore, A. Grinsted, and P.L. Woodworth (2008), Recent global sea level acceleration started over 200 years ago?, *Geophys. Res. Lett.*, *35*, L08715, doi:10.1029/2008GL033611.

Lambeck, K., and P. Johnston (1998), The viscosity of the mantle: Evidence from analyses of glacial rebound phenonena. In: *The Earth's Mantle* [I. Jackson (Ed.)], Cambridge University Press, pp. 461–502.

Lee, T.L., and D.S. Jeng (2002), Application of artificial neural networks in tide-forecasting, *Ocean Engineering*, *29*, 1003–1022, doi:10.1016/S0029-8018(01)00068-3

Mantua, N.J., S.R. Hare, Y. Zhang, J.M. Wallace, and R.C. Francis (1997), A Pacific interdecadal climate oscillation with impacts on salmon production. *Bull. Am. Meteorol. Soc.*, *78*, 1069–1079.

Mestas-Nuñez, A.M., and D.B. Enfield (1999), Rotated Global Modes of Non-ENSO Sea Surface Temperature Variability. *J. Clim.*, *12*, 2734–2746.

Milne, G. A., J. L. Davis, J. X. Mitrovica, H.-G. Scherneck, J. M. Johansson, M. Vermeer, and H. Koivula (2001), Space-geodetic constraints on glacial isostatic adjustment in

Fennoscandia. *Science*, *291*, 2381–2385.

Mitrovica, J. X. (2003), Recent controversies in predicting post-glacial sea-level change. *Quat. Sci. Rev.*, *22*, 127–133.

Müller, M.D., A.K. Kaifel, M. Weber, S. Tellmann, J.P. Burrows, and D. Loyola (2003), Ozone profile retrieval from Global Ozone Monitoring Experiment (GOME) data using a neural network approach (Neural Network Ozone Retrieval System (NNORSY)), *J. Geophys. Res.*, *108* (D16), 4497, doi:10.1029/2002JD002784

Nan, S., and J. Li (2003), The relationship between the summer precipitation in the Yangtze River valley and the boreal spring Southern Hemisphere annular mode, *Geophys. Res. Lett.*, *30* (24), 2266, doi:10.1029/2003GL018381

Parker, D.B. (1985), Learning Logic, Technical Report TR-47, *Center of Computational Research in Economics and Management Science*, MIT, Cambridge, MA

Parker, D., C. Folland, A. Scaife, J. Knight, A. Colman, P. Baines, and B. Dong (2007), Decadal to multidecadal variability and the climate change background, *J. Geophys. Res.*, *112* D18115, doi:10.1029/2007JD008411

Peltier, W.R. (2004), Global isostacy and the surface of the ice-age Earth: The ICE-5G (VM2) model and GRACE, *Ann. Rev. Earth Planet. Sci.*, *32*, 111–149, doi:10.1146/annurev.earth.32.082503.144359

Ponte, R. (1999), A preliminary model study of the large-scale seasonal cycle in bottom pressure over the global ocean, *J. Geophys. Res.*, *104*, 1289–1300.

Prandi, P., A. Cazenave, and M. Becker (2009), Is coastal mean sea level rising faster than the global mean? A comparison between tide gauges and satellite altimetry over 1993–2007, Geophys. Res. Lett., 36, L05602, doi:10.1029/2008GL036564.

Schöne, T., N. Schön, and D. Thaller (2009), IGS tide gauge benchmark monitoring pilot project (TIGA), scientific benefits. *J. Geod.*, *83*, 249–261, doi 10.1007/s00190-008-0269-y

Stammer, D., R. Tokmakian, A. Semtner, and C. Wunsch (1996), How well does a 1/4° global circulation model simulate large-scale oceanic observations?, *J. Geophys. Res.*, *101*, 25779–25811.

Stepanov, V.N., and C.W. Hughes (2006), Propagation of signals in basin-scale ocean bottom pressure from a barotropic model, *J. Geophys. Res.*, *111*, C12002, doi:10.1029/2005JC003450

Stogryn, A.P., C.T. Butler, and T. J. Bartolac (1994), Ocean surface wind retrievals from special sensor microwave imager data with neural networks, *J. Geophys. Res.*, *99* (C1), 981–984.

Tangang, F.T., W.H. Hsieh, and B. Tang (1998), Forecasting regional sea surface temperatures in the tropical Pacific by neural network models, with wind stress and sea level pressure as predictors, *J. Geophys. Res.*, *103* (C4), 7511–7522

Teferle, F.N., R.M. Bingley, S.D.P. Williams, T.F. Baker, and A.H. Dodson (2006) Using continuous GPS and absolute gravity to seperate vertical land movement and changes in sea-level at tide-gauges in the UK, *Phil. Trans. R. Soc. A*, *364*, 917–930, doi:10.1098/rsta.2006.1746.

Wenzel, M. (1993), Neural networks, a tool for prediction?, *Berichte aus dem Fachbereich Physik*, *Report 36*, Alfred-Wegener-Institute, Bremerhaven, Germany, pp.28

Wenzel, M., and J. Schröter (2007), The global ocean mass budget in 1993–2003 estimated from sea level change, *J. Phys. Oceanogr.*, *37(2)*, 203–213., doi:10.1175/JPO3007.1

Werbos, P. (1974), Beyond regression: New Tools for Prediction and Analysis in the Behavioral Science, *Ph.D. thesis*, Harvard, Cambridge, MA

White, N.J., J.A. Church, and J.M. Gregory (2005), Coastal and global sea level rise for 1950 to 2000, *Geophys. Res. Lett.*, *32*, L01601, doi:10.1029/2004GL021391

Woodworth, P.L., and R. Player (2003), The Permanent Service for Mean Sea Level: an update to the 21st century, *J. Coastal Res.*, *19*, 287–295.

Wöppelmann, G., B. M. Miguez, M.-N. Bouin, and Z. Altamimi, (2007), Geocentric sea-level trend estimates from GPS analyses at relevant tide gauges world-wide, *Glob. Planet. Change*, *57*, 396–406, doi:10.1016/j.gloplacha.2007.02.002

Wöppelmann, G., C. Letetrel, A. Santamaria, M.-N. Bouin, X. Collilieux, Z. Altamimi, S. D. P. Williams, and B. Martin Miguez (2009), Rates of sea-level change over the past century in a geocentric reference frame, *Geophys. Res. Lett.*, *36*, L12607, doi:10.1029/2009GL038720.

Table 1. Temporal RMS of the monthly differences for the regional mean sea level [cm/month] derived from the GFZ and the CSIRO altimeter products. *mean* = (GFZ+CSIRO)/2, *diff* = (CSIRO-GFZ) and *ratio* = *diff* / *mean*. See Fig. 2 for regions.

	dataset / signal RMS [cm/month]				
region	GFZ	CSIRO	*mean*	*diff*	*ratio*
trop. Indian	0.310	0.248	0.280	0.175	0.63
South	0.493	0.504	0.499	0.162	0.32
North	1.033	1.037	1.035	0.170	0.16
trop. Pacific	0.162	0.159	0.161	0.073	0.45
South	0.474	0.455	0.464	0.094	0.20
North	1.250	1.240	1.245	0.171	0.14
trop. Atlantic	0.272	0.243	0.258	0.092	0.36
South	0.529	0.535	0.532	0.101	0.19
global ocean	0.108	0.118	0.113	0.054	0.48

Table 2. Methods used to fill data gaps in tide gauge records (see text for details)

acronym	method
1: mac	mean annual cycle (MAC)
2: eof	EOF reconstruction (EOFR)
3: fc/recurr	FCnet, recurrent
4: fc/mac fill	FCnet with input gaps filled by MAC
5: fc/eof fill	FCnet with input gaps filled by EOFR
6: bc/recurr	BCnet, recurrent
7: bc/mac fill	BCnet with input gaps filled by MAC
8: bc/eof fill	BCnet with input gaps filled by EOFR
9: fc/bc best	best of 3 to 8 (minimal fore-/backcast error at known values)
10: fc/bc mean	error weighted mean of 3 to 8

Table 3. The effect of the choice of training data set on the regional mean sea level trend for the period 1900–2006. Given are the ensemble mean and standard deviation of the trends resulting from all C_r training values and applying the net to all tide gauge reconstructions (50 ensemble members). For the column *mean* the complete ensemble of trends (150 members) is taken into account. See Fig. 2 for regions.

Regional mean sea level trend , period: 1900–2006 [mm/yr]

region	training dataset GFZ	CSIRO	CSIRO+GFZ	*mean*
trop. Indian	1.30±0.55	0.21±0.79	0.45±0.63	0.65±0.81
South	-0.69±0.51	-0.85±0.77	-0.23±0.71	-0.59±0.72
North	2.68±1.12	3.62±1.14	3.44±1.20	3.25±1.22
trop. Pacific	1.47±0.44	2.64±0.35	1.55±0.31	1.89±0.65
South	1.43±0.57	0.85±0.60	1.41±0.65	1.23±0.66
North	3.25±1.01	3.86±0.89	4.01±1.27	3.70±1.11
trop. Atlantic	2.25±0.55	3.11±0.64	2.17±0.58	2.51±0.73
South	-0.35±0.80	0.26±0.61	0.10±0.77	0.00±0.77
global ocean	1.39±0.30	1.68±0.16	1.61±0.18	1.56±0.25

Table 4. The effect of the choice of training data set on the regional mean sea level acceleration for the period 1900–2006. Given are the ensemble mean and standard deviation of the accelerations resulting from all C_r training values and applying the net to all tide gauge reconstructions (50 ensemble members). For the column *mean* the complete ensemble of accelerations (150 members) is taken into account. See Fig. 2 for regions.

Regional mean sea level acceleration , period: 1900–2006 [mm/yr^2]

region	training dataset GFZ	CSIRO	CSIRO+GFZ	*mean*
trop. Indian	-0.0135±0.0088	-0.0015±0.0101	-0.0131±0.0078	-0.0094±0.0105
South	-0.0025±0.0092	0.0147±0.0088	0.0071±0.0084	0.0064±0.0112
North	-0.0007±0.0211	-0.0186±0.0192	-0.0150±0.0183	-0.0114±0.0209
trop. Pacific	-0.0047±0.0079	-0.0050±0.0075	-0.0069±0.0072	-0.0056±0.0076
South	0.0004±0.0123	0.0036±0.0085	0.0023±0.0113	0.0021±0.0108
North	0.0197±0.0221	0.0001±0.0185	0.0085±0.0203	0.0094±0.0218
trop. Atlantic	0.0148±0.0097	0.0105±0.0071	0.0091±0.0072	0.0115±0.0084
South	0.0203±0.0136	0.0247±0.0127	0.0249±0.0114	0.0233±0.0127
global ocean	0.0023±0.0049	0.0018±0.0033	0.0005±0.0044	0.0016±0.0043

Figure captions:

Figure 1. Layout of a backpropagation network (BPN) enriched by direct connections between the input and the output layer (indicated by the blue lines from the right).

Figure 2. The positions of the 56 selected tide gauges are marked by the red circles. The amount of monthly data available at these positions is indicated by the length of the corresponding vertical bars. The color shaded areas indicate the regions of interest in this paper.

Figure 3. Number of tide gauges with monthly data available.

Figure 4. Comparing the regional mean sea level anomaly (monthly differences) from the CSIRO (red) and the GFZ (green) dataset for (a) the tropical Pacific (15°S–15°N) and (b) the global ocean.

Figure 5. RMS error of the resulting recurrent backcast as compared with existing tide gauge values in dependence of the chosen ridge regression weight C_r (4). At each timestep the RMS values are normalized with the standard deviation of the corresponding known values, i.e. $Y = \left[\sum(y_k^{net} - y_k^{dat})^2 / \sum(y_k^{dat} - \overline{y^{dat}})^2\right]^{1/2}$. For better readability all curve are filtered to exclude the annual cycle.

Figure 6. Example for the resulting gap filling at the tide gauge Kwajalein (8.73°N 167.73°E, code 720011) using cases 1 to 8 from Table 2. The original data are shown in black.

Figure 7. RMS error of the resulting forecast (a) and backcast (b) as compared with existing tide gauge values. The error resulting from comparing the tide gauge data to the mean annual cycle are included in (a). The RMS values are normalized and filtered as in Fig. 5

Figure 8. Data part E_m of the TGRMnet costfunction (5) converted to a mean RMS value in dependence of the chosen C_r value and the six validation cases train 1 to train 6. The periods with data not used for training in cases train 1 to 5 are marked on the uppermost axis. For train

6 the retained data are chosen randomly from the whole period. Straight lines represent the cost from the training data and the dashed lines from the retained data. For comparison the data RMS and the data error (from Tab. 1) are included.

Figure 9. Reconstructed MSLA for the global ocean (a) and the North Pacific (b) resulting from the TGRMnet trained with CSIRO and with GFZ data compared to the training data (thin lines with marks). The mean from all C_r values and all tide gauge gap filling cases (Table 2) are shown. The CSIRO curve are offset by an arbitrary value.

Figure 10. Amplitude (a) and phase (b) of the annual cycle for the global MSLA from the CSIRO and the GFZ trained TGRMnet compared to the corresponding altimetric data (thin lines with marks).

Figure 11. Regional MSLA for the different ocean regions (color shaded areas in Fig. 2) in dependence of the training data chosen for the network training. For each training dataset the mean of the corresponding regional MSLA sub-ensemble (5 C_r values times 10 tide gauge reconstructions) is shown. The black line and grey shading give the mean and standard deviation, respectively, of the complete ensemble (150 members). For the global ocean (a) the results from *Church and White* [2006] and from *Jevrejeva et al.* [2006] are included for comparison. NOTE: All curves are filtered before plotting to eliminate the annual cycle!

Figure 12. Ensemble mean regional sea level anomaly for the different ocean regions after removing the annual cycle and the quadratic regression. The global ocean and the Indian are shown in (a), the Pacific in (b) and the Atlantic in (c).

Figure 13. Amplitude (a, b, c) and phase (d, e, f) of the annual cycle for the regional MSLA: global ocean and Indian Ocean are given in (a) and (d), the Pacific is in (b) and (e) and the Atlantic in (c) and (f). Amplitude and phase are estimated by fitting an annual period sinusoid

to the high-passed filtered ensemble mean MSLA curves (150 members) within a moving 5 year window, wherein the corresponding values are given at its center. Phases are given as date of maximum value.

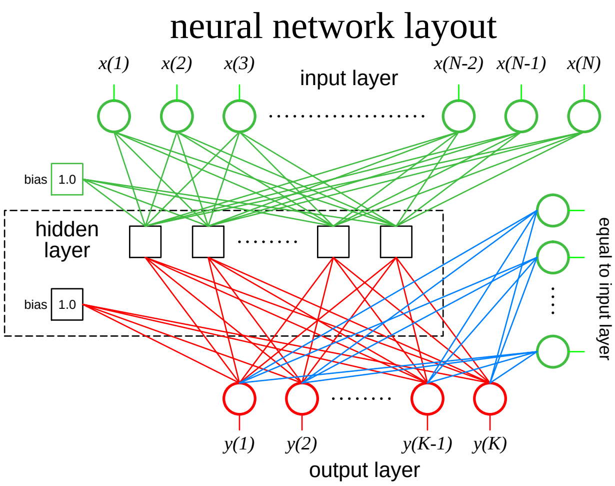
neural network layout
x(1)
x(2)
x(3)
input layer
x(N-2)
x(N-1)
x(N)
bias
1.0
hidden layer
bias
1.0
equal to input layer
y(1)
y(2)
y(K-1)
y(K)
output layer

Figure 1.

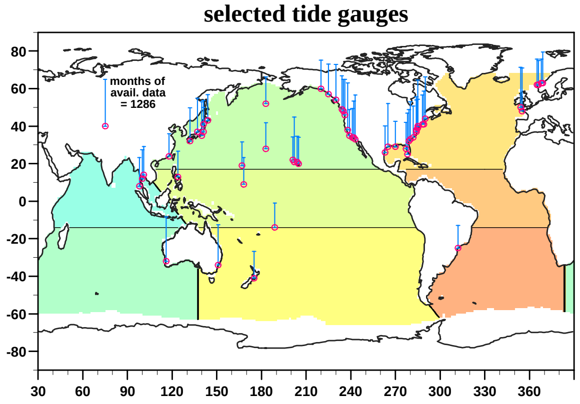

Figure 2.

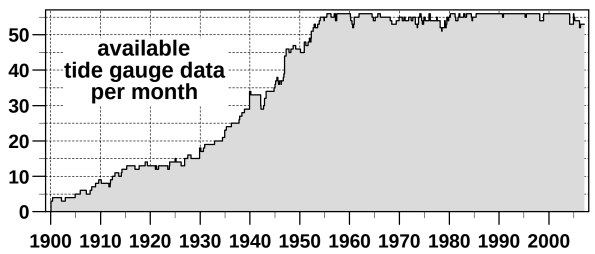

Figure 3.

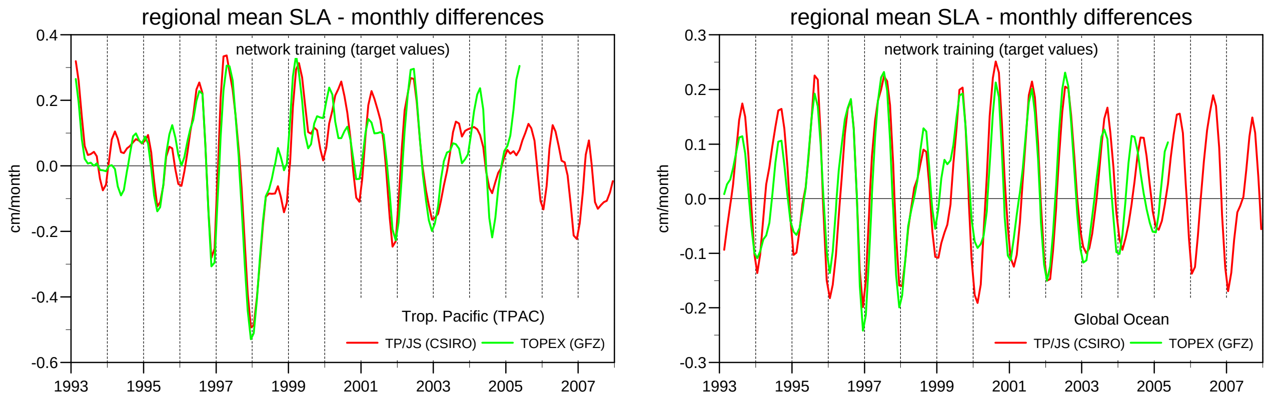

Figure 4.

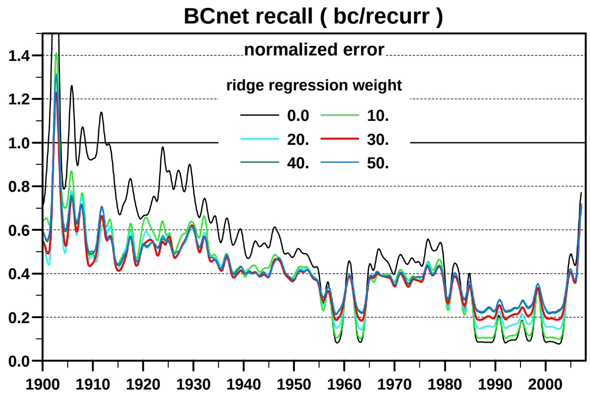

Figure 5.

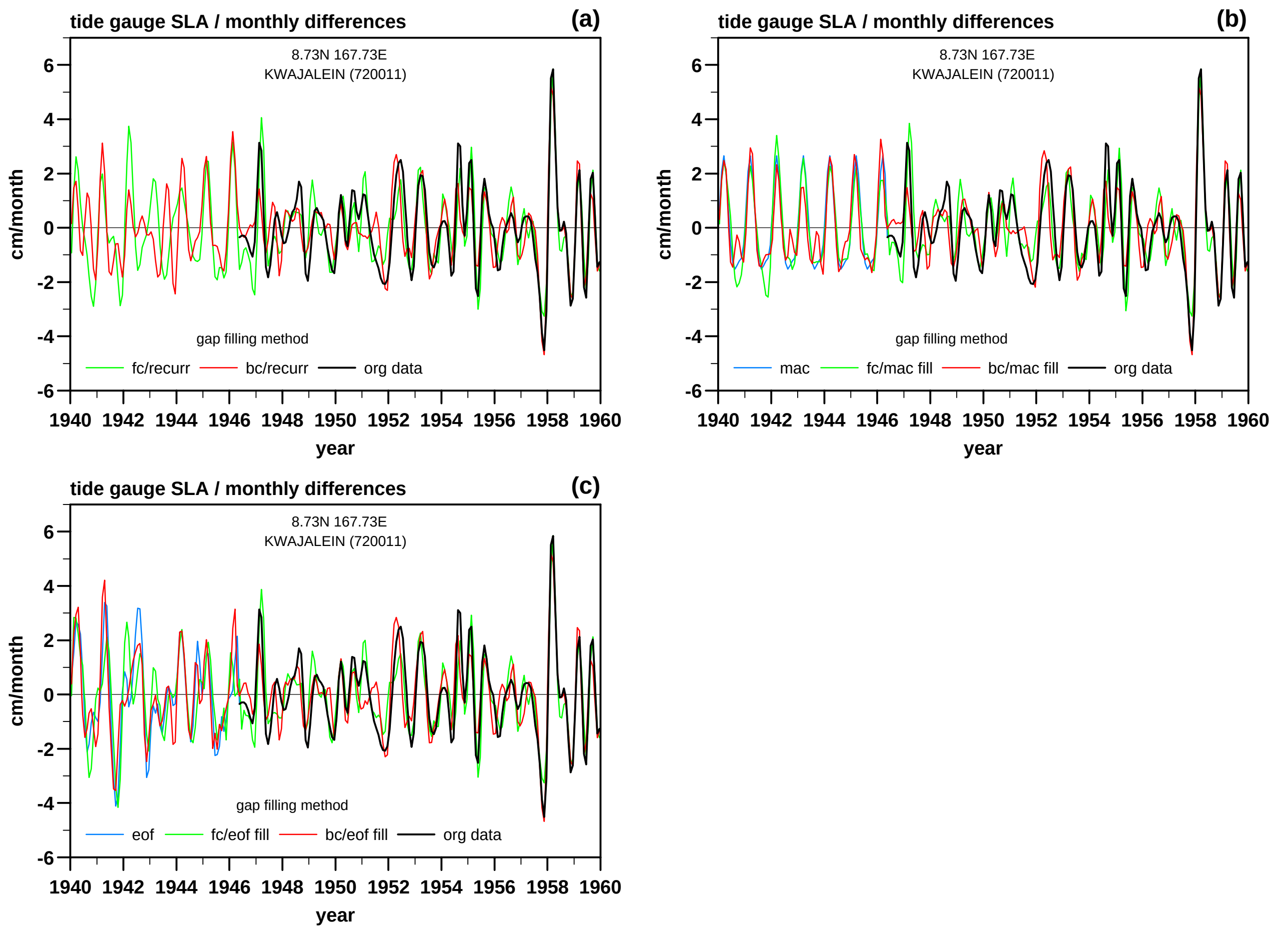

Figure 6.

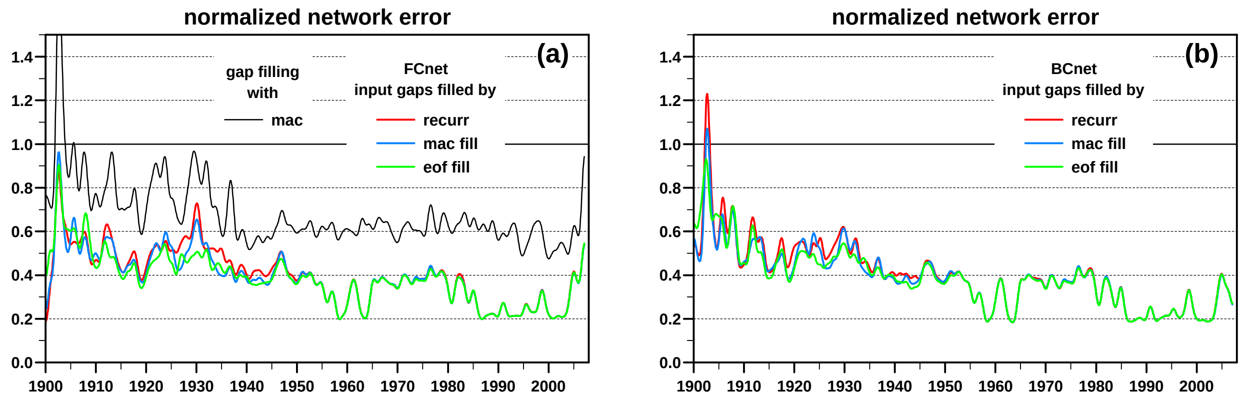

Figure 7.

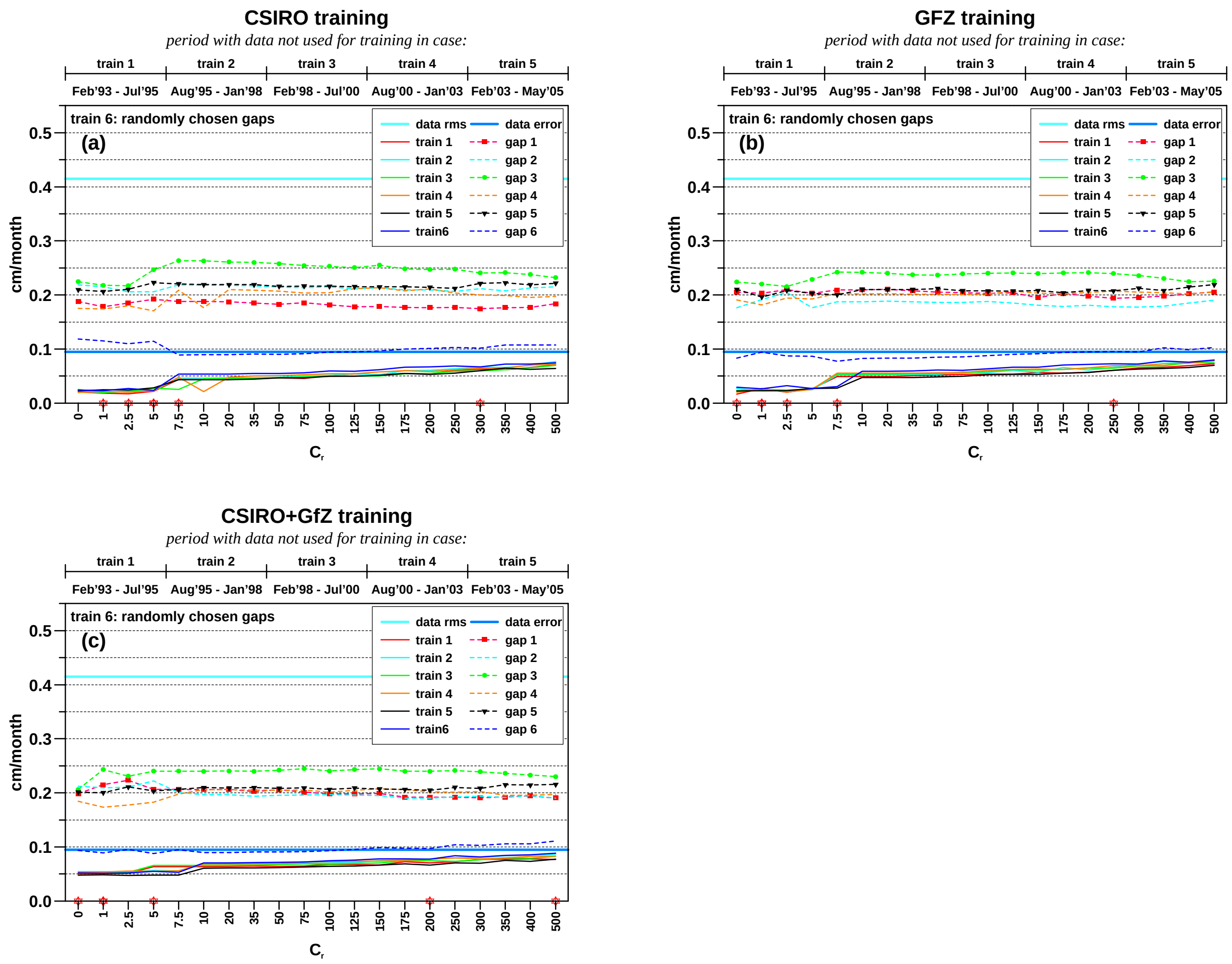

Figure 8.

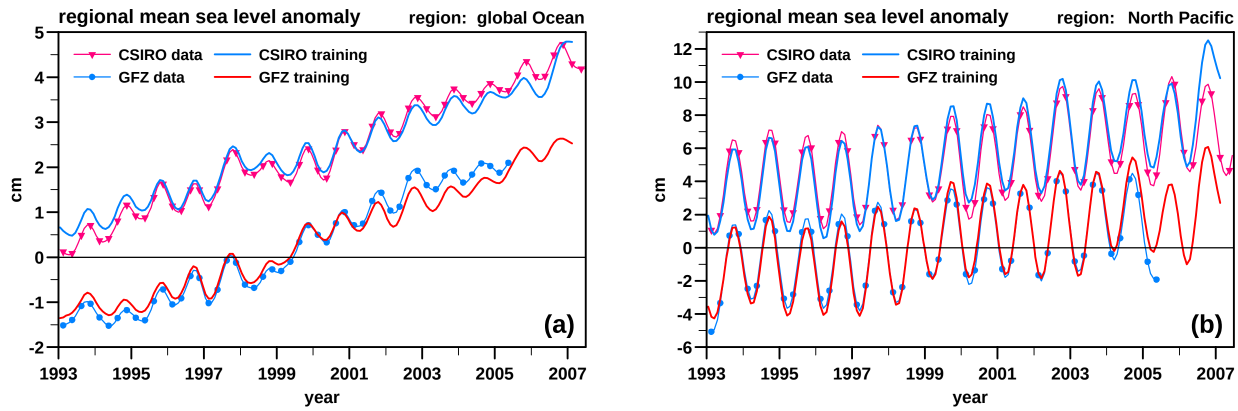

Figure 9.

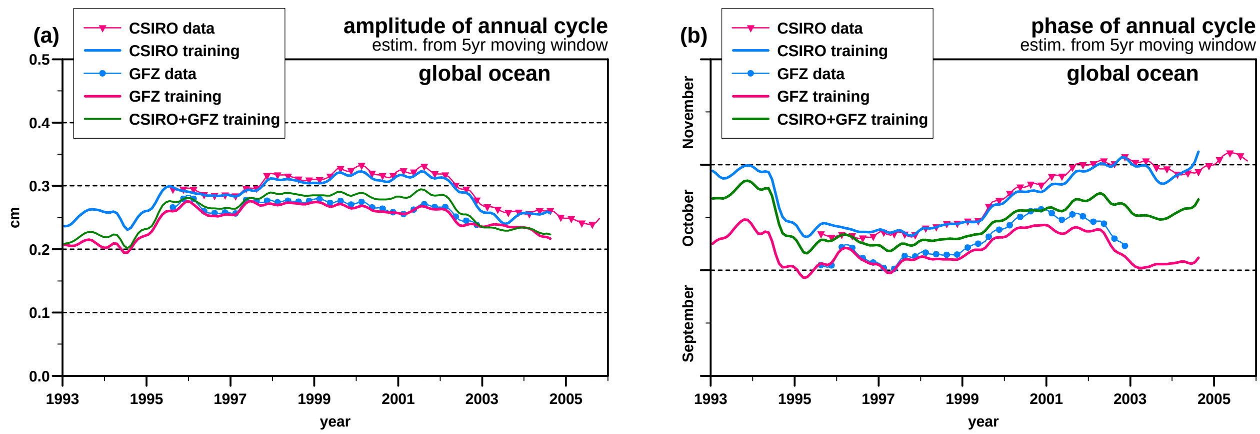

Figure 10.

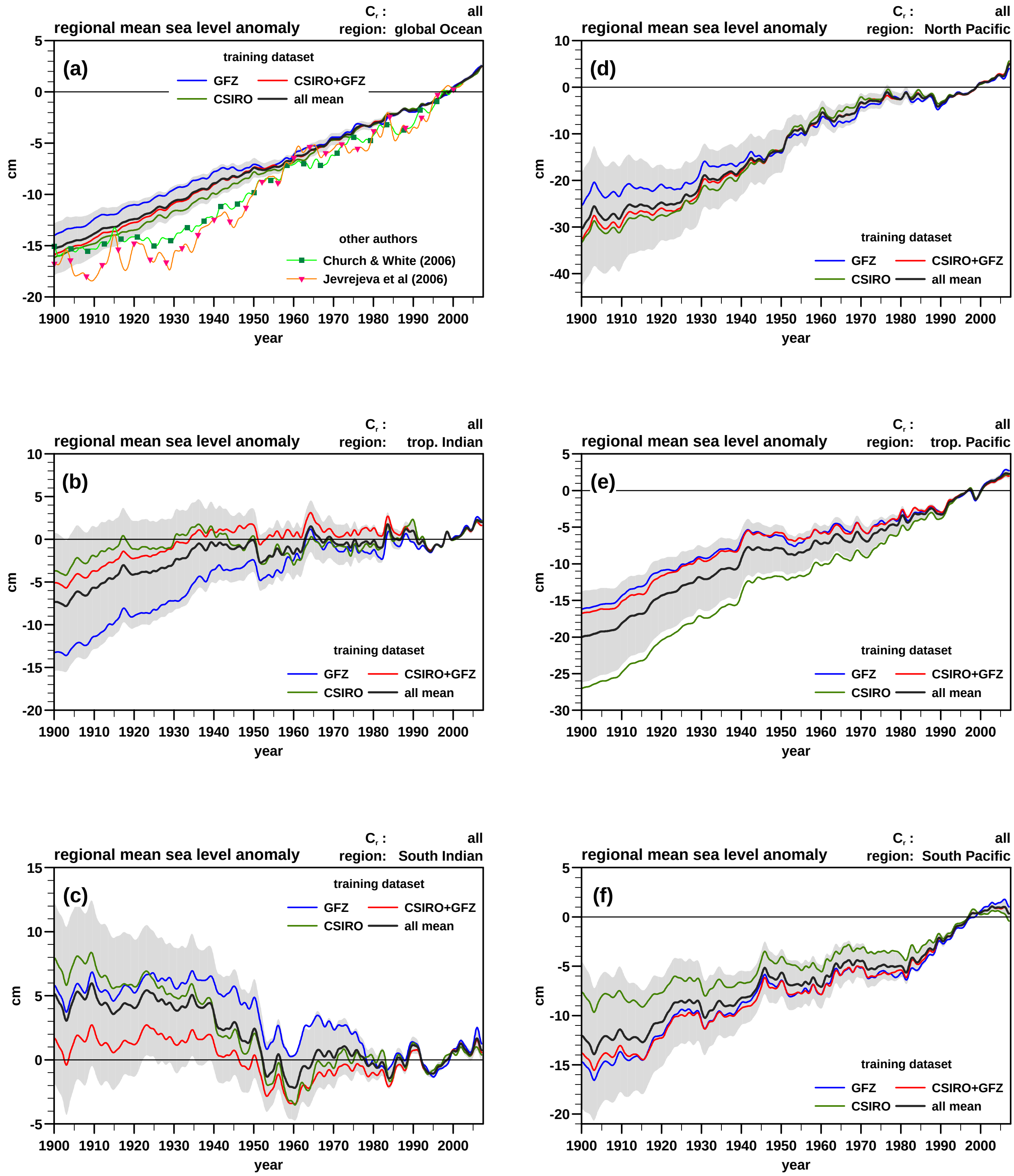

Figure 11. ... continued on next page!

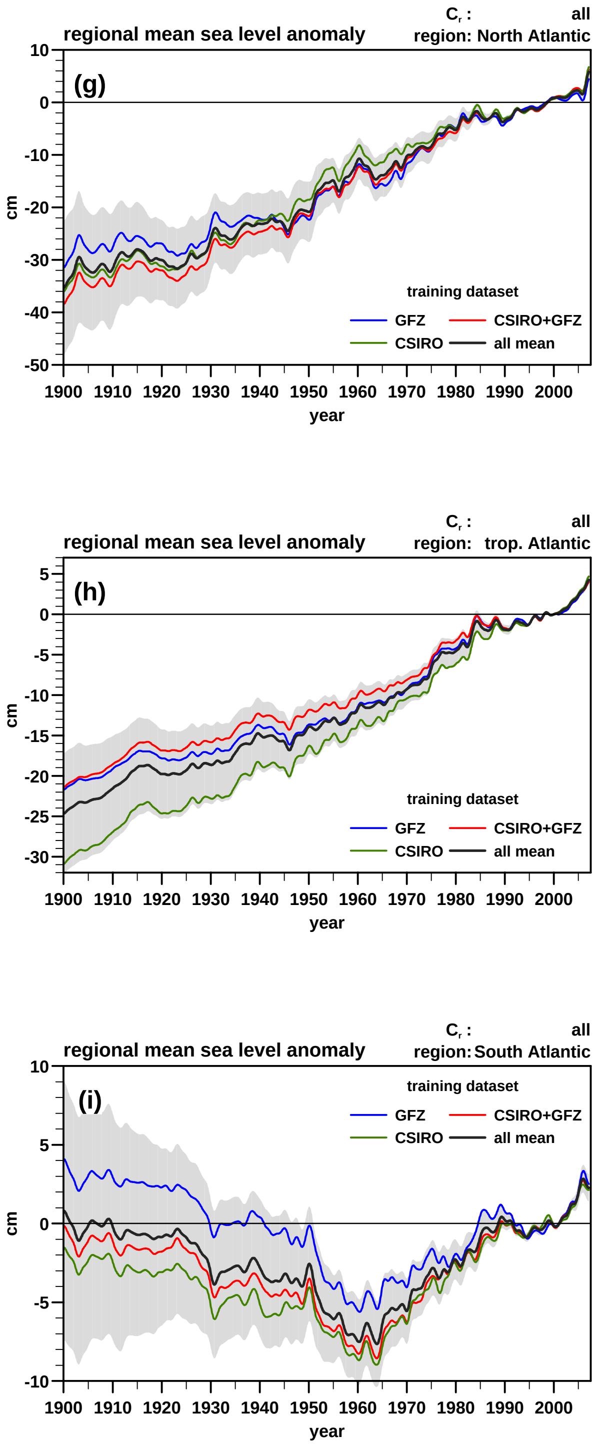

Figure 11. ... continued

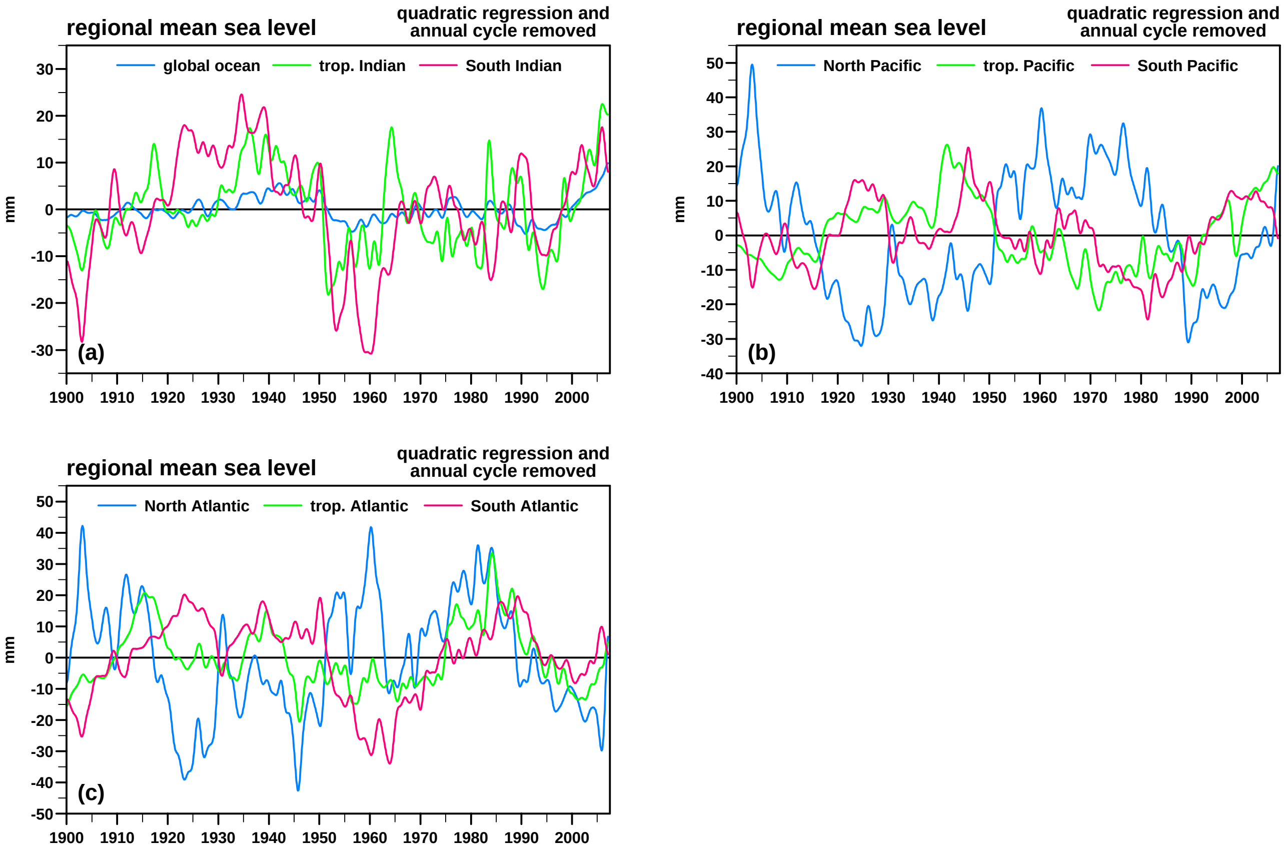
regional mean sea level
quadratic regression and annual cycle removed
global ocean
trop. Indian
South Indian
mm
(a)
North Pacific
trop. Pacific
South Pacific
(b)
North Atlantic
trop. Atlantic
South Atlantic
(c)
1900 1910 1920 1930 1940 1950 1960 1970 1980 1990 2000

Figure 12.

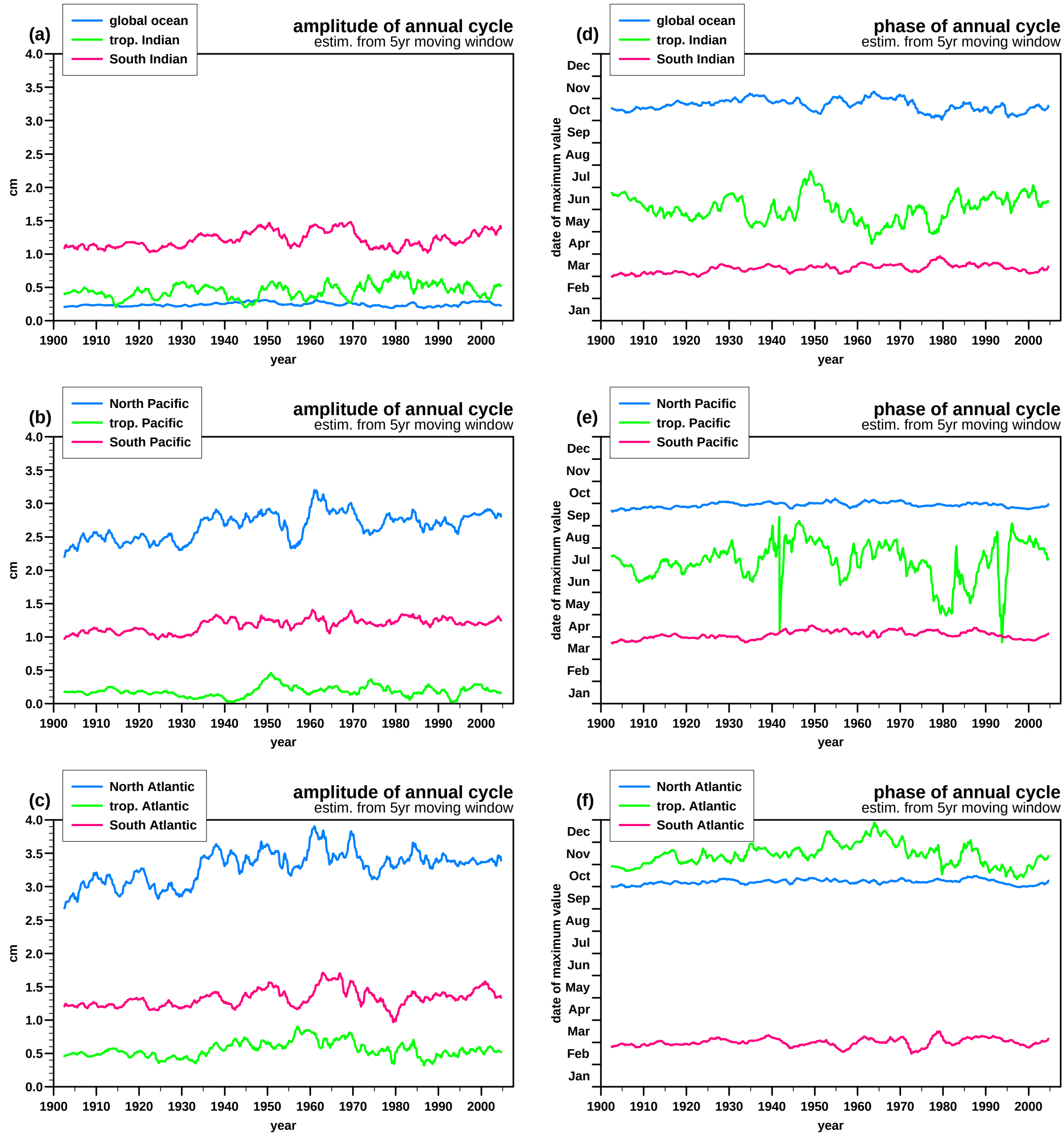
(a)
global ocean
trop. Indian
South Indian
amplitude of annual cycle
estim. from 5yr moving window
cm
year
(b)
North Pacific
trop. Pacific
South Pacific
amplitude of annual cycle
estim. from 5yr moving window
(c)
North Atlantic
trop. Atlantic
South Atlantic
amplitude of annual cycle
estim. from 5yr moving window
(d)
phase of annual cycle
estim. from 5yr moving window
date of maximum value
Jan
Feb
Mar
Apr
May
Jun
Jul
Aug
Sep
Oct
Nov
Dec
(e)
phase of annual cycle
estim. from 5yr moving window
(f)
phase of annual cycle
estim. from 5yr moving window

Figure 13.